

A Sequential Generalized Likelihood Ratio Test for Signal Detection from Photon Counting Images

MENGYA (MIA) HU,^{1,*} HE SUN,² ANTHONY HARNESS,¹ AND N. JEREMY KASDIN³

¹ *Department of Mechanical and Aerospace Engineering, Princeton University, Princeton, NJ, 08544, USA*

² *Department of Computing and Mathematical Sciences, California Institute of Technology, Pasadena, CA, 91125, USA*

³ *College of Arts and Sciences, University of San Francisco, San Francisco, CA, 94117, USA*

* mengyah@princeton.edu

Abstract: Exoplanets are very dim. An Electron Multiplying Charged Coupled Device (EMCCD) operating in photon counting (PC) mode reduces the noise level and enables their detection. Typically, PC images are added together as a co-added image before processing. We present here a signal detection and estimation technique working directly with the PC images. The method is based on the generalized maximum likelihood ratio test (GLRT) and uses a binomial distribution between PC images. It can be applied online, so it is possible to stop observations once we have reached a threshold confidence for the existence (or absence) of planets, and thus the observation time is efficiently used. It directly uses the detector model, which more accurately represents its noise characteristics. We show that it outperforms our previous GLRT method using co-added images under Gaussian noise assumption.

© 2022 Optical Society of America under the terms of the [OSA Open Access Publishing Agreement](#)

1. Introduction

Direct imaging of exoplanets is challenging; the flux ratio between an Earth-like exoplanet and its sun-like host star is around 10^{-10} at visible wavelengths [1]. A starshade or internal coronagraph can suppress the starlight and leave only the planet's light to be detected, however, the planets are extremely faint and detecting them is still a challenge. An Earth-like planet ranges from 28th to 30th magnitude or fainter. As a result, the signal can be smaller than the read noise. EMCCDs can alleviate this problem by amplifying the signal in an electron-multiplication (EM) register, thus reducing the effective readout noise to less than one electron [2]. Unfortunately, at the same time, it introduces a new noise – the multiplicative noise from the amplification process. This can be overcome by operating in photon counting (PC) mode. PC Mode reports a value of 1 or 0 in each pixel for each integration time by thresholding the value at the final stage. The value reported in the pixel is one if the number of electrons in a pixel is bigger than a chosen threshold and zero otherwise. The binary value only indicates the existence of photons in the pixels during the integration time but does not reveal the exact number of those photons. Examples of simulated PC images are shown in Fig. 1 (all the simulations mentioned in this work use a 1 second integration time) and the details about how we simulate the images can be found in our previous paper [3]. To utilize the photons efficiently, we need to choose the exposure time so that the expected photon count in any pixel is much less than one.

Operation of an EMCCD in photon counting mode is fairly new and thus still developing. Available literature on the design and characteristics of EMCCD detectors can be found in Refs. 4–8. Previous work on image processing focuses mainly on image stacking and Bayesian estimation methods [9, 10], which are applied to co-added PC images rather than designed for individual PC images [11, 12]. As those methods generally require a high signal-to-noise-ratio,

large numbers of PC images are needed, which takes a long observation time. In our previous work, we presented an alternative methodology for co-added PC images [13], which can efficiently detect even weak signals automatically. However, all these methods do not provide theoretical guidance on how to choose the integration times and the total number of PC images to combine into one co-added image.

In this work, we utilize a statistical model for the EMCCD to obtain a relationship between the detection probability and the photon rate. We use this distribution to formulate a binomial distribution for the values of the same pixel on different PC images. Then, sequential detection and estimation is performed. Within hundreds of seconds, detection and accurate intensity estimation can be achieved. We begin this paper with a description of the detector model, followed by the methodology of the sequential GLRT, and an application example. Finally, we compare the performance of our previous method, GLRT using co-added images [13], and this sequential GLRT method using PC images directly. This work builds on our previous work introduced in Ref. 14.

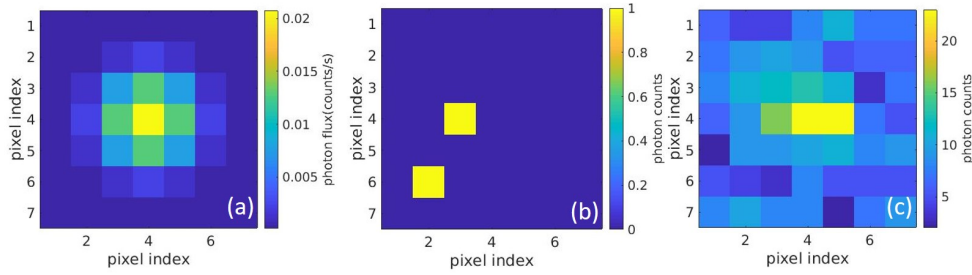


Fig. 1. (a) Simulated point spread function (PSF) for the Wide Field Infrared Survey Telescope (WFIRST) with a $1e-8$ Jy light source, 0.021 arcsec/pixel. (b) A photon counting (PC) image of (a) with 1s integration time. (c) A co-added image from 780 sequential PC images.

2. A Stochastic Model for EMCCDs in Photon Counting Mode

Hirsch et al. present a detailed imaging process for an EMCCD and build a statistical model for each stage of the imaging process [2]. First, incident photons follow a Poisson process. Second, the EM register is represented by a gamma distribution. Third, readout noise is added using a Gaussian distribution. Hirsch et al. use some approximations to simplify and arrive at the equation for the probability distribution for the number of electrons:

$$\lambda = s \times q \times t + d \times t + CIC \quad (1)$$

$$p(n_{ic}) = \begin{cases} \frac{1}{\sqrt{2\pi}\sigma} \exp(-\lambda - \frac{n_{ic}^2 - B_{PC}}{2\sigma^2}) + \frac{2}{g} F_{\chi}(2\lambda; 4, \frac{2n_{ic}}{g}), & n_{ic} > 0 \\ \frac{1}{\sqrt{2\pi}\sigma} \exp(-\lambda - \frac{n_{ic}^2 - B_{PC}}{2\sigma^2}), & \text{otherwise,} \end{cases} \quad (2)$$

where λ is the expected number of input electrons for the EM register, s is the photon rate, q is the quantum efficiency (units are shown in Table 1), t is the integration time, d is the dark current, CIC is the clock induced charge, n_{ic} is the number of counts after the EM register, including readout noise, $p(n_{ic})$ is the probability of counts n_{ic} , σ is the standard deviation of the readout noise, g is the EM gain, B_{PC} is the bias in PC mode, $F_{\chi}(2\lambda; 4, \frac{2n_{ic}}{g})$ is the non-central χ^2 distribution for 2λ with 4 degrees of freedom and the non-centrality parameter $\frac{2n_{ic}}{g}$.

Finally, a threshold is applied to get a final binary result. Combining models for all the stages described above produces the final model, which calculates the probability of getting a value of 1

on the detector given a certain incident intensity. Thus, with a threshold of $B_{PC} + T \times \sigma$, the probability of detecting a one value is:

$$f(s, t) = \int_{B_{PC} + T \times \sigma}^{\infty} p(n_{ic}) dn_{ic}. \quad (3)$$

The value in each pixel in each image only has two outcomes: either 1 or 0; the probability of getting a value of 1, $f(s, t)$, is decided by the integration time, t , and the ground-truth of the flux, s . As the integration time and the flux in each pixel is fixed, the probability is fixed. That is to say, the measurement in each pixel in each image satisfies a Bernoulli distribution and the measurements for the same pixel in different images satisfy a Binomial distribution. In this paper, we assume a fixed integration time, so $f(s, t)$ is simplified to $f(s)$. That is to say, for each pixel, the imaging result follows a Bernoulli distribution, whose probability of value 1 is related to the intensity of flux in the pixel. Fig. 2 shows results for the detection probability given different flux levels and the derivative of this probability calculated in Mathematica. We use the detector parameters values shown in Table 1, which are similar to the parameter values of WFIRST [15] and assume a starshade for starlight suppression. The detection probability increases as the flux increases, where a very small flux or a very large flux tend to give deterministic zero or one measurements. The binary value only indicates the existence of photons in the pixels during the integration time but does not reveal the exact number of the photons. To utilize the photons efficiently, we need to choose the exposure time so that the expected photon count in any pixel is less than 1.

Parameter	Symbol	Value	Unit
Quantum efficiency	q	1	ph/e^-
Integration time	t	1	s
Clock-induced charge	CIC	0.01	$e^- pixel^{-1} frame^{-1}$
Dark current	d	2×10^{-4}	$e^- pixel^{-1} s^{-1}$
Electron-multiplying gain	g	2500	—
PC Bias	B_{PC}	200	$e^- pixel^{-1} frame^{-1}$
Standard deviation of readout noise	σ	100	$e^- pixel^{-1} frame^{-1}$
Threshold Parameter	T	5.5	—

Table 1. EMCCD detector parameters

3. Sequential Generalized Likelihood Ratio Test

The Generalized Likelihood Ratio Test is a powerful tool for detection. Our previous work approximated the noise in the co-added images by Gaussian distributions [13]. In this work, we use the more accurate probability function derived in the previous section. As a result, measurements in each pixel in each image follow a Bernoulli distribution, while measurements in the same pixel for several sequential images follow a binomial distribution.

3.1. Signal Estimation

We begin with the simple model of the signal received by the detector,

$$s = \alpha PSF + \beta, \quad (4)$$

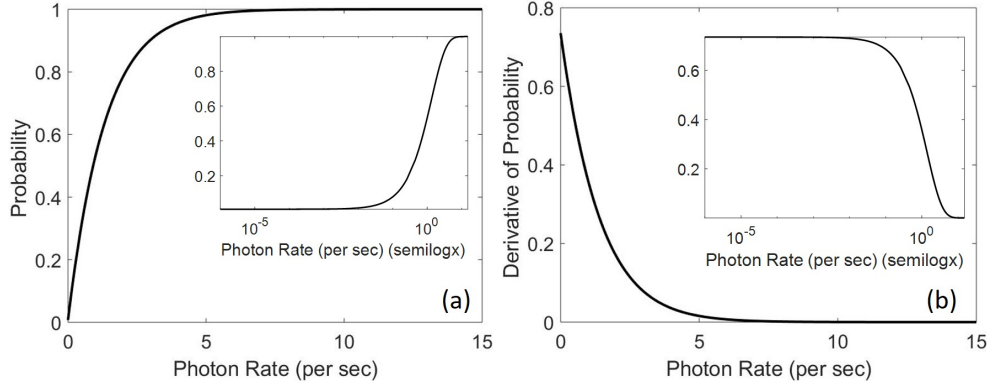


Fig. 2. Detection probability and its derivative. (a) Detection probability as a function of photon flux, $f(s)$ calculated by Eq. (3), where s is in units of photons per second. (b) Derivative of the detection probability. The insets are the same plots shown with a logarithmic abscissa.

where \mathbf{PSF} is a reference point spread function (PSF) of the telescope; α is the scale factor between the planet intensity and the source intensity of the PSF; and β is the background light (such as dust and light leakage from starshade defects). We stack pixel values in the target area into a column vector for easier mathematical manipulation. That is to say, s and \mathbf{PSF} are column vectors. Given the PSF shape, $\mathbf{PSF} = (x_1, \dots, x_K)^T$, where the subscripts of x represent the pixel indices and K is the total number of samplings in a PSF, the conditional probability of N measurements, $\mathbf{y} = \{y_1, \dots, y_N\}$, can be written as

$$p(\mathbf{y}|\alpha, \beta) = \prod_k^K f(\alpha x_k + \beta)^{N_{1,k}} [1 - f(\alpha x_k + \beta)]^{N_{2,k}}, \quad (5)$$

where $N_{1,k}$ and $N_{2,k}$ respectively represent the frequency of one and zero occurring in N measurements of the k -th pixel. The equality $N = N_{1,k} + N_{2,k}$ holds for every pixel. Taking the natural logarithm of both sides of Eq. (5), the log-likelihood of the series of measurements is

$$L(\alpha, \beta) = \sum_k^K N_{1,k} \ln[f(\alpha x_k + \beta)] + N_{2,k} \ln[1 - f(\alpha x_k + \beta)]. \quad (6)$$

To estimate α and β , we can conduct a maximum likelihood estimation (MLE) based on Eq. (6) by taking the derivatives with respect to α and β and setting them equal to zero,

$$\begin{aligned} \frac{\partial L(\alpha, \beta)}{\partial \alpha} &= N \sum_k^K x_k f'(\alpha x_k + \beta) \frac{N_{1,k} - N f(\alpha x_k + \beta)}{N f(\alpha x_k + \beta) [1 - f(\alpha x_k + \beta)]} = 0, \\ \frac{\partial L(\alpha, \beta)}{\partial \beta} &= N \sum_k^K f'(\alpha x_k + \beta) \frac{N_{1,k} - N f(\alpha x_k + \beta)}{N f(\alpha x_k + \beta) [1 - f(\alpha x_k + \beta)]} = 0, \end{aligned} \quad (7)$$

These equations can be solved for estimates of α and β using a gradient descent method. As can be seen, the derivatives are weighted summations of the difference between the measurements and the distribution means, where $N f(\cdot)$ and $N f(\cdot)[1 - f(\cdot)]$ are respectively the mean and variance (the series of measurements follows a binomial distribution, since each measurement satisfies a Bernoulli distribution), and $f'(s) = df(s)/ds$. According to Fig. 2 (b), the function $f'(s)$ is zero

when $s \rightarrow +\infty$. That means that the method neglects the difference between different intensities that are too large in the estimation since the photon counting detector always gives 1 in these cases.

3.2. Signal Detection

The detection of an exoplanet signal can be modeled as a composite hypotheses testing problem. The null and alternative hypotheses are as follows:

$$\begin{aligned} H_0 : \alpha = 0, \beta \geq 0 \\ \text{versus} \\ H_1 : \alpha > 0, \beta \geq 0. \end{aligned} \quad (8)$$

Here, since we have no prior information about the exoplanet intensity α , and the background light β , we can conduct a generalized likelihood ratio test (or also called maximum-likelihood test), i.e., we determine whether there is an exoplanet signal based on the ratio

$$R = \frac{\max_{\alpha, \beta} p_1(\mathbf{y}|\alpha, \beta)}{\max_{\alpha, \beta} p_0(\mathbf{y}|\alpha, \beta)} = \frac{\max_{\alpha, \beta} \prod_k^K f(\alpha x_k + b)^{N_{1,k}} [1 - f(\alpha x_k + b)]^{N_{2,k}}}{\max_{\beta} \prod_k^K f(\beta)^{N_{1,k}} [1 - f(\beta)]^{N_{2,k}}}, \quad (9)$$

where $p_0(\cdot)$ and $p_1(\cdot)$ are the probability under hypothesis H_0 and H_1 , respectively, and the two maximal probabilities and the corresponding parameters (α and β) are calculated using the estimation algorithm in Sec. 3.1. In a real space mission, we can conduct sequential detection while sequentially collecting images. After getting every new image, we update the test ratio in Eq. (9); when $R \geq \pi_U$ or $R \leq \pi_L$, we conclude H_1 or H_0 is accepted and stop taking new images, otherwise we take a new image and repeat the detection procedure, where π_U and π_L are thresholds chosen beforehand. The thresholds are determined according to our desired true positive or false alarm rates.

3.3. Multi-signal Detection in an Image

The hypothesis testing process described in the previous section assumes the planet PSF is exactly in the center of the set of K test pixels. In reality, an image much bigger than the size of a PSF will be examined for an unknown numbers of planets in an unspecified location. Thus, the detection procedure is repeated for each set of pixels across the whole image. This generates a log-likelihood ratio map for the image. As we will see in the example in the next section, the pixel where the planet is located has a high log-likelihood ratio value, and the pixels within a PSF size range around this center pixel also have high log-likelihood ratio values compared to the background. This makes sense as an image window centered on any of them presents a bright partial signal. Our methods only consider two cases. The first is that a signal is at the center of the window. The second one is that no signal exists in the window (only constant background). Therefore, the bright partial signal will have a high log-likelihood ratio as it is close to Hypothesis 1. However, it does not follow Hypothesis 1, so the log-likelihood ratio is lower than that in the real signal pixel. Thus, we will just choose the convex areas with high log-likelihood ratio values and the center of its circumscribed circle as the position of the planet. This planet position estimation should be more robust, especially when only a partial signal is in the image. Our method detects the existence of the signals quickly and separates them from the background successfully. The more observations, the more confidence we gain for the detection.

3.4. Case Study

We simulate a signal with intensity $1e-8$ Jy (for reference, Venus is $2.99e-8$ Jy; Earth is $4.85e-9$ Jy) and run multiple trials to get the statistics of our method's performance, shown in Fig. 3. Our

method correctly estimates the intensity of the signal quickly. The value of the log-likelihood ratio is high and increases quickly with the increasing number of observations. It means that we can confidently detect the existence of a signal with just a few images and the more observations the more confidence we gain for the detection.

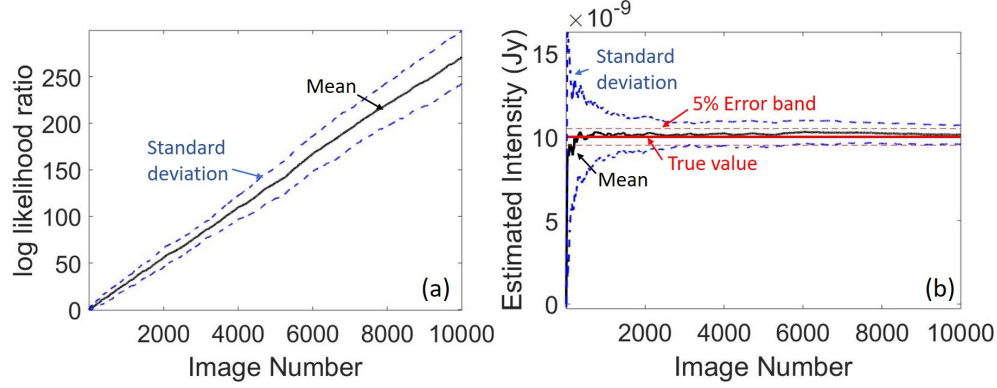


Fig. 3. Statistics of the maximum likelihood planet intensity estimation from 70 trials. The black solid line is the average of all trials with an increasing number of observations and the blue dashed lines are the sample standard deviation band. (a) The log-likelihood ratio with an increasing number of observations. The more images we have, the bigger the log-likelihood ratio is. Thus, we have more confidence of the existence of a true signal. (b) The estimated intensity with increasing number of images. The red solid line is the true intensity. The red dashed lines are the 5% error band. The blue dashed line is the standard deviation band. The method gives a good estimate.

We apply the method described in the above sections to simulate starshade images to detect possible exoplanet signals. As shown in Fig. 4 (a), we observe our solar system from 10 pc away with a Starshade-WFIRST system, where two observable planets are in view, Venus and Earth. Here we use a fixed integration time, one second, for each single exposure. More details about the simulation are available in our previous paper [3]. It is hard to show all PC images one by one here, so to give a sense of what the data look like, the co-added images are shown in Figs. 4 (b), (d), (f) and (h). Their corresponding log-likelihood ratio maps are shown in Figs. 4 (c), (e), (g) and (i). The change of log-likelihood ratio at Venus, Earth and a background pixel after each observation are shown in Fig. 5. As the figures demonstrate, our method can detect the existence of the signals quickly and separate them from the background successfully. The more observations, the more confidence we gain for the detection.

3.5. Comparison with GLRT under a Gaussian Assumption

We introduced a GLRT method in our previous paper [13]. The method there works for co-added images and assumes Gaussian distributions for the noise. In comparison, the new sequential GLRT introduced in this paper works for single PC images. It is easier to use online, as it can process a new PC image and we only need to update the detection metrics R in Eq. (9) by multiplying it with the likelihood ratio from the new image rather than recomputing all the values. More importantly, it uses a binomial distribution rather than Gaussian. The underlying relationship between the probability in the binomial distribution and flux intensity can be derived theoretically based on the detector model or directly measured in experiment. No approximation is used. It is very accurate and thus the method is very efficient at extracting information.

To demonstrate the different properties of the two methods, we compare their ROC curves for the detection of Venus and Earth. It is hard to analytically derive a closed form relationship

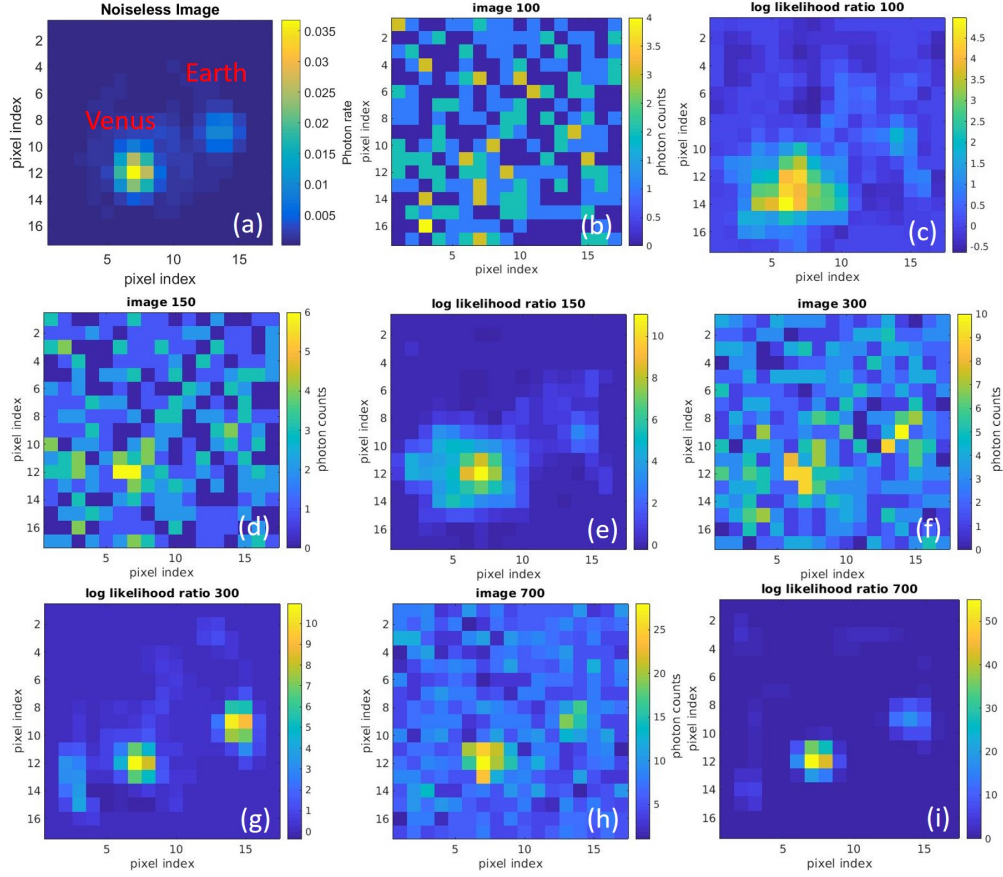


Fig. 4. Our new Binomial based GLRT can determine the existence of a planet or lack thereof efficiently. (a) Simulated Noiseless image for the solar system from 10 pc away with Starshade-WFIRST system. This is the ground-truth for the detection problem. (b) Co-added image with 100 sequential PC images for Fig.4(a). (c) False alarm rate of each pixel using the 100 sequential PC images in Fig.4(b). (d) Co-added image with 150 sequential PC images for Fig.4(a). (e) False alarm rate of each pixel using the 150 sequential PC images in Fig.4(d). (f) Co-added image with 300 sequential PC images for Fig.4(a). (g) False alarm rate of each pixel using the 300 sequential PC images in Fig.4(f). (h) Co-added image with 700 sequential PC images for Fig.4(a). (i) False alarm rate of each pixel using the 700 sequential PC images in Fig.4(h). The change of Log likelihood ratio of Venus, Earth and a background pixel with increasing number of observations is shown in Fig 5.

between the false alarm rate and true positive rate and the threshold chosen in the new Binomial based sequential GLRT, compared to our previous GLRT [13], which assumes Gaussian noise. Thus, we use Monte Carlo simulations to calculate the receiver operating characteristic (ROC) curves, shown in Fig. 6. For Fig. 6(a), we ran 5000 trials with 20 PC images generated for Venus and Earth in each trial. Sequential GLRT was applied to the 20 PC images and Gaussian GLRT was applied to the co-added image of the 20 PC images. Results for different decision thresholds were recorded and combined into the ROC curve. For Fig. 6(b), we ran 2500 trials and 200 PC images for each trial. As Venus is brighter than Earth, the performance for Venus is better than Earth when we use the same method and the same number of PC images. The performance for

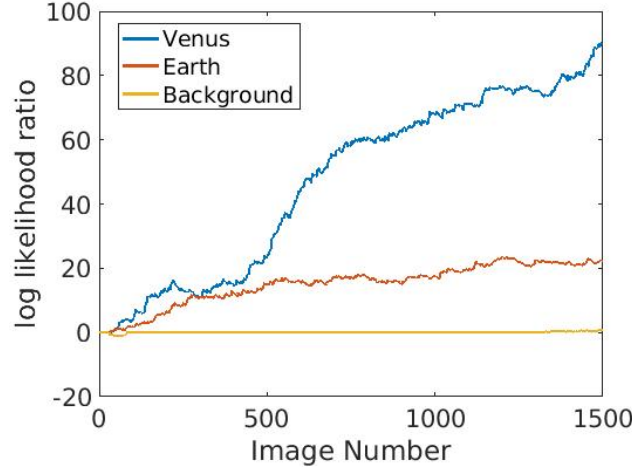


Fig. 5. Log likelihood ratio of Venus, Earth and a background pixel (5th row, 5th column) with increasing number of observations for Fig.4(a) using Binomial based sequential GLRT.

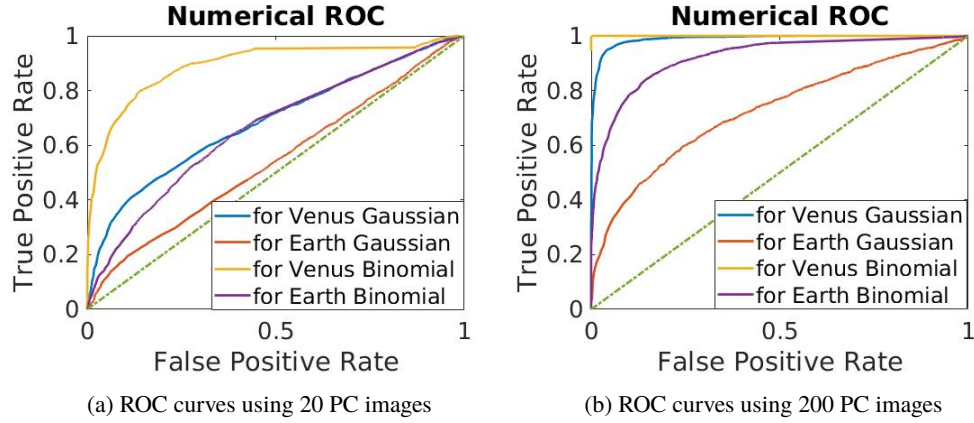


Fig. 6. Receiver operating characteristic curves for Earth and Venus detection with the two different methods. ‘Gaussian’ in the legends means the result used the previous GLRT [13], which processes co-added images and assumes white noise. ‘Binomial’ means the result used the sequential GLRT described in this paper, which directly processes PC images. (a) ROC curves using 20 PC images. (b) ROC curves using 200 PC images.

both Venus and Earth using either method is better with more images. It is easy to understand that the method performs better with more information, i.e. more images. Furthermore, the sequential GLRT outperforms our previous method.

4. Conclusions

In this paper we presented a model and signal processing approach based directly on single photon counting images. Previous work on PC image processing is mainly applied to co-added PC images rather than designed for individual PC images. All these methods do not provide theoretical guidance on how to choose the total number of PC images to combine into one

co-added image. Our method here directly works with each PC image, so we do not need to worry about choosing the hyper parameter, number of PC images, to combine into one co-added image. Furthermore, previous work on PC image processing assumes Gaussian noise for co-added images, but the method here directly uses the detector model, which more accurately represents its noise characteristics. In this paper, we show that it outperforms our previous GLRT method using co-added images under Gaussian noise assumption.

This approach maximizes the utilization of information presented in each observation. We applied this method to simulated starshade images and successfully detected Venus and Earth. Directly processing the PC images online helps allocate the observation time efficiently. We can compare the log-likelihood ratio with thresholds chosen beforehand after each observation and stop accordingly. As we can decide the existence or lack of planet efficiently in this way, we can move to other planetary systems if there is no planet or make sure that enough information is gathered if there is a planet.

Funding

This work is supported by Caltech-JPL NASA grant NNN12AA01C.

References

1. W. A. Traub and B. R. Oppenheimer, *Exoplanets* (University of Arizona Press, Tucson, 2011).
2. M. Hirsch, R. Wareham, M. Martin-Fernandez, M. Hobson, and D. Rolfe, "A stochastic model for electron multiplication charge-coupled devices—From theory to practice," *PLOS One* **8**, e53671 (2013).
3. M. Hu, A. Harness, Y. Kim, N. J. Kasdin, R. Vanderbei, M. Rizzo, and A. Roberge, "Simulation of realistic images for starshade missions," in *Techniques and Instrumentation for Detection of Exoplanets VIII*, vol. 10400 of *Proc. SPIE* (2017), p. 104001S.
4. G. A. de Vree, A. H. Westra, I. Moody, F. van der Have, K. M. Ligtoet, and F. Beekman, "Photon-counting gamma camera based on an electron-multiplying ccd," *IEEE Transactions on Nucl. Sci.* **52**, 580–588 (2005).
5. M. C. DeSantis, S. H. DeCenzo, S. H. Li, and Y. M. Wang, "Precision analysis for standard deviation measurements of immobile single fluorescent molecule images," *Opt. express* **18**, 6563–6576 (2010).
6. C. Mackay, T. Staley, D. King, F. Suess, and K. Weller, "High-speed, photon-counting ccd cameras for astronomy," in *High Energy, Optical, and Infrared Detectors for Astronomy V*, vol. 7742 of *Proc. SPIE* (2010), p. 774202.
7. O. Daigle, O. Djazovski, D. Laurin, R. Doyon, and E. Artigau, "Characterization results of emccds for extreme low-light imaging," in *High Energy, Optical, and Infrared Detectors for Astronomy V*, vol. 8453 of *Proc. SPIE* (2012), p. 845303.
8. A. N. Wilkins, M. W. McElwain, T. J. Norton, B. J. Rauscher, J. F. Rothe, M. Malatesta, G. M. Hilton, J. R. Bubeck, C. A. Crady, and D. J. Lindler, "Characterization of a photon counting emccd for space-based high contrast imaging spectroscopy of extrasolar planets," in *High Energy, Optical, and Infrared Detectors for Astronomy V*, vol. 9154 of *Proc. SPIE* (2014), p. 91540C.
9. E. Lantz, J. L. Blanchet, L. Furfaro, and F. Devaux, "Multi-imaging and bayesian estimation for photon counting with emccds," *Mon. Notices Royal Astron. Soc.* **386**, 2262–2270 (2008).
10. K. B. W. HarpsÅye, M. I. Andersen, and P. Kjøgegaard, "Bayesian photon counting with electron-multiplying charge coupled devices (emccds)," *Astron. & Astrophys.* **537**, A50 (2012).
11. C. A. G. Gonzalez, O. Wertz, O. Absil, V. Christiaens, D. Defrere, D. Mawet, J. Milli, P. A. Absil, and M. V. Droogenbroeck, "Vip: Vortex image processing package for high-contrast direct imaging," *The Astron. J.* **154**, 7 (2017).
12. R. Soummer, L. Pueyo, and J. Larkin, "Detection and characterization of exoplanets and disks using projections on karhunen-loÅve eigenimages," *The Astrophys. J. Lett.* **755**, L28 (2012).
13. M. Hu, A. Harness, and N. J. Kasdin, "Image processing methods for exoplanets detection and characterization in starshade observations," in *Space Telescopes and Instrumentation 2018: Optical, Infrared, and Millimeter Wave*, vol. 10698 of *Proc. SPIE* (2018), p. 106985K.
14. M. Hu, H. Sun, and N. J. Kasdin, "Sequential generalized likelihood ratio test for planet detection with photon-counting mode," in *Techniques and Instrumentation for Detection of Exoplanets IX*, vol. 11117 of *Proc. SPIE* (2019), p. 111171K.
15. M. J. Rizzo, N. T. Z. T. D. Groff, Q. Gong, A. M. Mandell, P. Saxena, M. W. McElwain, A. Roberge, J. Krist, A. E. Riggs, and E. J. Cady, "Simulating the wfirst coronagraph integral field spectrograph," in *Techniques and Instrumentation for Detection of Exoplanets VIII*, vol. 10400 of *Proc. SPIE* (2017), p. 10400B.